



Distinct contributions of meprins to skin regeneration after injury – Meprin α a physiological processor of pro-collagen VII



Daniel Kruppa^{a,b1}, Florian Peters^{c,d1}, Olivier Bornert^a, Mareike D. Maler^{a,b}, Stefan F. Martin^a, Christoph Becker-Pauly^c and Alexander Nyström^{a*}

a - Department of Dermatology, Faculty of Medicine and Medical Center – University of Freiburg, Germany

b - Faculty of Biology, University of Freiburg, Freiburg, Germany

c - Biochemical Institute, Christian-Albrechts-University Kiel, Germany

d - Laboratory for Retinal Cell Biology, Department of Ophthalmology, University Hospital Zurich, University of Schlieren / Zurich, Schlieren, Zurich, Switzerland

Correspondence to Alexander Nyström:*Dep. of Dermatology, Faculty of Medicine, Medical Center – University of Freiburg, Hauptstr. 7, 79104 Freiburg, Germany (Alexander Nyström). alexander.nystroem@uniklinik-freiburg.de (A. Nyström)

<https://doi.org/10.1016/j.mbplus.2021.100065>

Abstract

Astacin-like proteinases (ALPs) are regulators of tissue and extracellular matrix (ECM) homeostasis. They convey this property through their ability to convert ECM protein pro-forms to functional mature proteins and by regulating the bioavailability of growth factors that stimulate ECM synthesis. The most studied ALPs in this context are the BMP-1/tolloid-like proteinases. The other subclass of ALPs in vertebrates – the meprins, comprised of meprin α and meprin β – are emerging as regulators of tissue and ECM homeostasis but have so far been only limitedly investigated. Here, we functionally assessed the roles of meprins in skin wound healing using mice genetically deficient in one or both meprins. Meprin deficiency did not change the course of macroscopic wound closure. However, subtle but distinct contributions of meprins to the healing process and dermal homeostasis were observed. Loss of both meprins delayed re-epithelialization and reduced macrophage infiltration. Abnormal dermal healing and ECM regeneration was observed in meprin deficient wounds. Our analyses also revealed meprin α as one proteinase responsible for maturation of pro-collagen VII to anchoring fibril-forming-competent collagen VII *in vivo*. Collectively, our study identifies meprins as subtle players in skin wound healing.

© 2021 Published by Elsevier B.V. This is an open access article under the CC BY-NC-ND license (<http://creativecommons.org/licenses/by-nc-nd/4.0/>).

Introduction

The preservation of healthy skin is dependent on balanced turnover of the majority of its proteome at regular intervals [1,2]. Here, extracellular matrix (ECM) proteins are no exceptions; compromised balanced replacement of spent or functionally deficient ECM proteins with fresh copies occurs in, and may also be causal of, conditions spanning from age-related skin fragility to fibrosis [3,4]. After trauma to the skin such as wounding, the normal

fine-tuned turnover is temporarily replaced by healing-stage-dependent shifts in the synthesis and degradation balance. Failure to progress through this transient imbalance of the ECM underlies chronic wounds and scarring [5].

Extracellular proteinases are crucially involved on both ends to achieve homeostasis of the dermal ECM. They remove damaged proteins but also regulate synthesis and protein deposition by controlling release of active growth factors and by converting lesser biologically active pro-forms to

mature, active ECM proteins. Members of the astacin-like family of metalloendopeptidases (ALPs) are notable players in the latter context. In mammalian skin they comprise the BMP-1/tolloid-like proteinases (BTPs) and the meprins. BMP-1, mTLD, TLL1 and TLL2 belong to the BTPs and the meprins comprise meprin α and meprin β . In the skin, all but TLL2 appears to be expressed at biologically relevant levels [6–9].

For regulation of ECM production and deposition the BTPs have been considerably more investigated than the meprins. Although, BTPs may promote ECM gene expression through cleavage of latent TGF β -binding or TGF β -activating proteins facilitating subsequent release of active TGF β [10,11], they are most known for their ability to process and mature structural ECM proteins, in particular collagen precursors. BTPs may control all major steps of dermal collagen fibrillogenesis [9,12–15]. Importantly, BTPs release the N- and C-termini of laminin-332 and the C-terminus of pro-collagen VII [8,16], both are core constituents of the dermal-epidermal junction (DEJ) that are essential for skin integrity [17].

Deletion of *Bmp1/mTld* (*Bmp1* and *mTld* are splice variants of the same gene [18]) and *Tll1* in adult murine skin results in thin and fragile skin with abnormal collagen fibrillogenesis and retention of fibrillar pro-collagens [9]. Histologically the collagen matrix appears more compacted and the average diameter of individual collagen fibrils is reduced. Wound healing of combined *Bmp1/mTld* and *Tll1* deficient skin is significantly impaired with slower re-epithelialization and impaired granulation tissue formation [9].

The aforementioned study as well as other investigations have also indicated that other proteinases can, to some extent, perform similar actions as BTPs in skin [8,9]. Given the conservation of the catalytic domains between meprins and BTPs, meprins would be candidates to at least partially contribute to such activities. Indeed, they cut the laminin $\gamma 2$ chain of laminin-332 [19] and have been identified to be able to process C propeptide of collagen I and III [7,20] at distinct cleavage sites including those used for BMP-1. Additionally, meprins can also release the N propeptide of collagen I and III [7,20], thus they possess the ability to fully mature collagen I and III.

BTPs and meprins share a preference for an acidic residue at the P1' position [21]. However, the substrate repertoire for meprins appears broader, they are also more catalytically active and do not require enhancer proteins for efficient removal of pro-collagen C-propeptide [22]. Meprins not only act as activators of proteins but can also be inactivators [22]. Meprin α and meprin β are encoded by the *MEP1A* and *MEP1B* genes, respectively. They are synthesized as pro-forms that require activation by tryptic proteinases including kallikreins, plasmin and trypsin [22]. Meprins exist

as membrane-bound forms or shed into the microenvironment by furin-mediated release of meprin α during the secretory pathway or by ADAM10 and 17-mediated release of meprin β at the cell surface [19,23,24]. Interestingly, meprin β can induce activity of ADAM10 and 17, indicating a close relationship between these proteinases [25]. In contrast to BTPs, meprins can form homo- or hetero-dimers or even larger complexes in the case of meprin α [22,26].

Apart from maturing ECM proteins, meprins are closely linked to regulation of inflammation [27]. Meprins may stimulate inflammatory responses through e.g. activation of interleukin (IL)-1 β , IL-18 and through shedding of IL-6 and IL-11 receptor ectodomains promoting trans-signaling [27–29]. However, they may also suppress inflammation through inactivation of IL-6 and CCL2 [27,30]. Collectively, this makes the outcomes of inflammation modulation by meprins complex and contextual.

Both meprins are expressed in skin [6,7,20]. In healthy human epidermis meprin α is most abundant in the basal layer and meprin β is present in the granular layer [6]. In hyperproliferative hyperkeratotic conditions this patterning is broken and wider epidermal distribution of meprins occurs [6]. Additionally, the abundance of meprins in healthy human dermis appears low but a marked increase of meprin α has been observed in keloid scars [7]. Support of dermal activities of meprins comes from abnormal collagen fibril formation and thinning of dermis occurring in meprin α and meprin β deficient mice [20].

To functionally assess the roles of meprins in skin from injury to re-establishment of homeostasis, we carefully followed wound healing in mice with single or combined meprin deficiency. Our data indicate that meprins have modest but distinct roles during skin wound healing. Complete absence of meprin delays re-epithelialization and reduces macrophage infiltration in wounds. Meprin α appears to play the most prominent role in dermal ECM regeneration. Notably, our studies disclose meprin α as a physiological processor of pro-collagen VII.

Results

Meprins are minor ALPs of the skin

Meprins had previously been described to be expressed in skin [6,7]; however, their relative expression in skin to the other class of ALPs the BTPs had not been determined. Toward this end, we examined gene expression in human epidermal keratinocytes and dermal fibroblasts of all six ALPs – BMP1 (*BMP1*), mTLD (*mTLD*), TLL1 (*TLL1*), TLL2 (*TLL2*), meprin α (*MEP1A*) and meprin β (*MEP1B*).

In accordance with previous studies [8], *BMP1* and *mTLD* were the major BTPs expressed in

human skin cells (Fig. 1A); significantly lower but specific expression of *TLL1* and *TLL2* was observed in both human keratinocytes and fibroblasts (Fig. 1A). Compared to *BMP1* and *mTLD* the gene expression of both meprins in keratinocytes and fibroblasts was substantially lower (Fig. 1A). *MEP1B* was significantly higher expressed than *MEP1A* in both keratinocytes and fibroblasts (Fig. 1B), whereas both cell types expressed meprins at similar levels (Fig. 1B). These observations differ from previous reports but align with recent RNAseq data [7,31].

Next, in order to find a suitable *in vivo* model that could be used for translational interrogation of the roles of meprins in skin, we analyzed ALP expression and meprin distribution in murine wild-type (WT) skin. As in human, *Bmp1/mTld* was

the most abundantly expressed BTP (Fig. 1C). Low expression of both meprins was detected (Fig. 1C). Importantly, staining of murine tail skin for meprin α and meprin β revealed similar epidermal distribution as in healthy human skin [6]. Meprin α was most abundant basal and spinous layers and meprin β being present in more superficial layers (Fig. 1D). Furthermore, specific staining for meprin α was seen in the dermis (Fig. 1D arrows). This was again similar to human skin where meprin α but not meprin β is detected in healthy dermis [7]. Collectively, these analyses show conserved expression profiles and distribution of meprins in human and murine skin. Thus, mouse represents a suitable animal model for translational assessment of meprin function in skin.

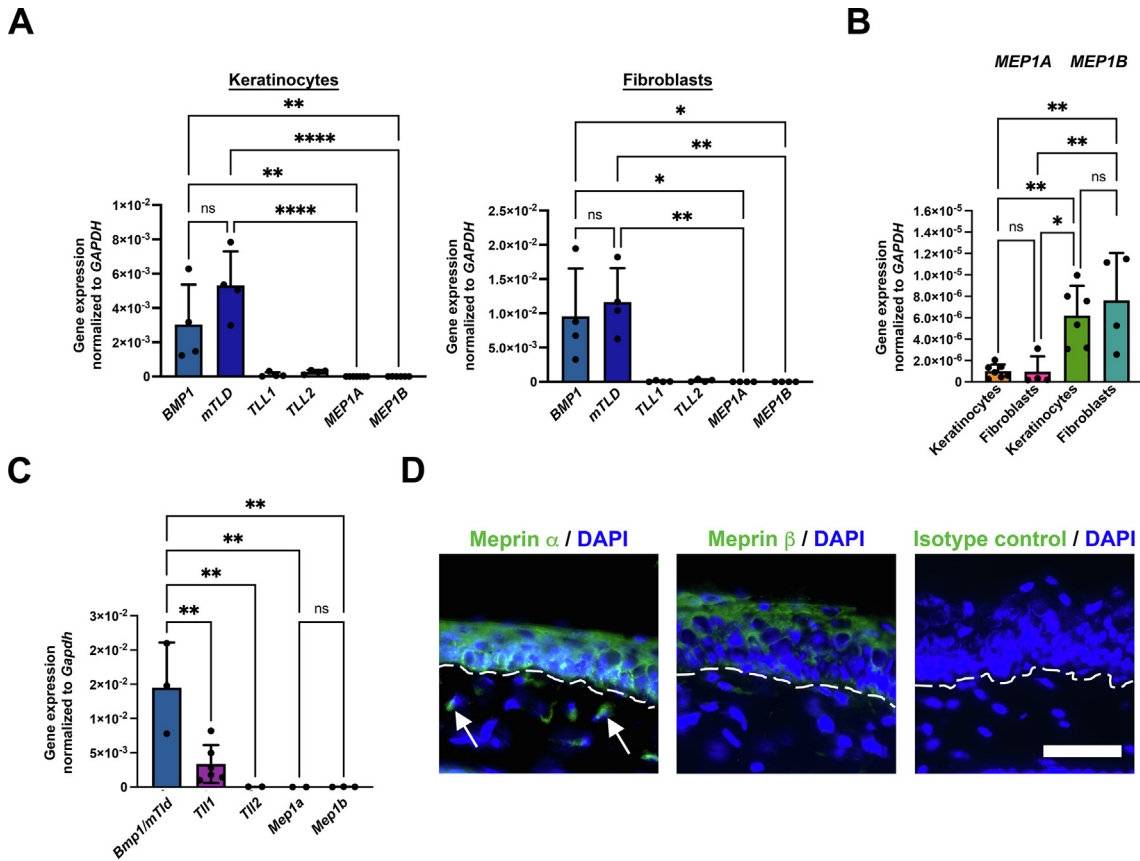


Fig. 1. ALP expression in human skin cells and murine skin. A, Gene expression of ALPs in human epidermal keratinocytes and dermal fibroblasts analyzed by real-time qPCR. B, Values from analyses in A shown for *MEP1A* and *MEP1B* Kera, keratinocytes; Fibro, fibroblasts. C, Murine adult WT back skin analyzed for ALP gene expression by real-time qPCR. D, Staining of murine WT tail skin for meprin α and meprin β discloses similar distribution as previously reported for human skin [6], localization of meprin α primarily to basal and spinous layers and meprin β primarily to granular layers of keratinocytes. In addition meprin α is seen in the dermis (arrows), also similar to previous staining of healthy human skin [7]. Nuclei were counterstained with DAPI (blue). Rabbit pre-immune sera was used as isotype (Iso) control. Scale bar = 50 μ m. A–C, individual values from different donor cells ($n = 4-7$), mean \pm S.D. are shown, * $P < 0.05$; ** $P < 0.01$; *** $P < 0.001$; **** $P < 0.0001$ as analyzed by one-way ANOVA with Tukey’s correction. (For interpretation of the references to colour in this figure legend, the reader is referred to the web version of this article.)

Macroscopic wound healing progresses with normal rate in meprin deficient skin

Skin of meprin single or double deficient mice appears macroscopically normal. Challenges are often needed to reveal functions of proteins for which some redundancy and compensation occur. Given their association with inflammation and ECM maturation, alongside reported increased abundance of meprins in selected fibrotic disease, wound healing was deemed as a relevant challenge for meprin deficient skin. Staining for meprins in WT mouse skin wounds confirmed that meprins were dynamically present in epidermal tongues. At day 3 meprin α was abundant in the epidermal tongues, whereas meprin β was lowly present. After re-epithelialization had been achieved and epidermal differentiation occurred, meprin α became more confined to the basal and spinous layers and

meprin β abundance re-emerged in the more superficial epidermal layers (Fig. 2A). At day 7 they were also present in granulation tissue (Fig. 2A).

Following the confirmation of dynamic expression of meprins during wound healing, 7-week-old WT mice and mice with single or combined meprin deficiency were punched with a 6 mm punch biopsy tool through a skin fold, creating two wounds per mouse. Macroscopically, the wounds closed with a largely similar speed for all genotypes (Fig. 2B and C). However, careful analysis of the raised wound tissue disclosed that in *Mep1a*^{-/-} mice the healed wounds needed significantly fewer days to flatten and return to the level of surrounding unwounded skin (Fig. 2D).

Combined meprin deficiency slows wound re-epithelialization

Next, we performed histological analyses. These revealed reduced epidermal coverage in 3-day-old

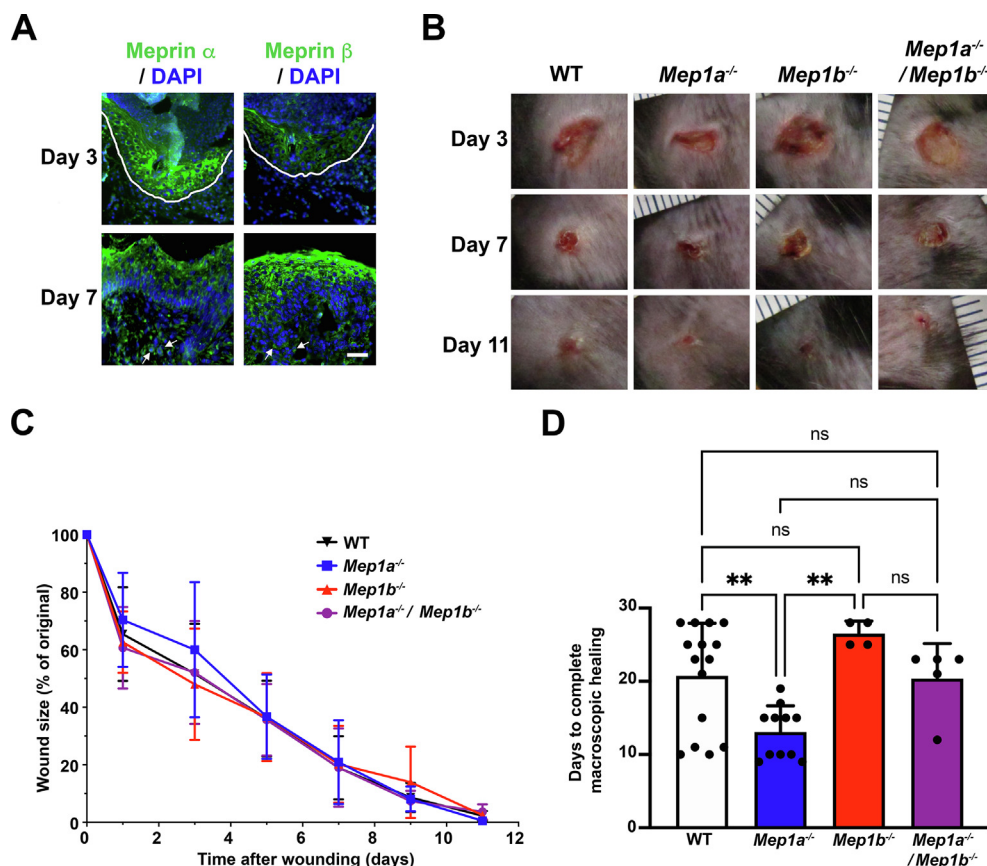


Fig. 2. Meprins are expressed in healing murine wounds and their absence does not alter the speed of macroscopic wound closure. A, 3- and 7-day-old dorsal skin wounds from WT mice stained for meprin α and meprin β . Drawn white line indicates epidermal tongue and arrows show meprin positivity in granulation tissue. Nuclei were counterstained with DAPI (blue). Scale bar = 50 μ m. B, Photographs of the same wounds in WT, *Mep1a*^{-/-}, *Mep1b*^{-/-}, and combined *Mep1a*^{-/-}/*Mep1b*^{-/-} 3, 7 and 11 days after wounding. C, Graph showing macroscopic wound closure for a total of 18 wounds per genotype. Values represent mean \pm S.D. D, The quantification shows the days after wounding until re-leveling of the raised wound to the level of the surrounding unwounded skin occurred. Individual values for individual wounds (n = 4–15), mean \pm S.D. are shown, ***P* < 0.01 as analyzed by one-way ANOVA with Tukey's correction. (For interpretation of the references to colour in this figure legend, the reader is referred to the web version of this article.)

wounds with combined meprin deficiency (Fig. 3A and B). This reduced re-epithelialization was due to shortened epidermal tongues (Fig. 3A). It was a transient delay and by day 7 all analyzed wounds from all genotypes were fully covered with new epidermis (Fig. 3A). Furthermore, single or combined meprin deficiency had no obvious influence on differentiation of the newly formed epidermis (Supplemental Fig. S1A).

After wounding downregulation of E-cadherin normally occurs in epidermal tongues and forced overexpression of E-cadherin delays re-epithelialization [32,33], indicating that loss of E-cadherin increases the mobility of cells. E-cadherin has been identified in *in vitro* studies as a substrate of meprin β [34]. Cleavage of E-cadherin by meprin β evokes E-cadherin degradation and reduces cell-cell adhesion [34]. Therefore, we analyzed wounds of different ages (3 and 7 days) for E-cadherin appearance. For all genotypes, E-cadherin was present at very low level in day 3 wound epidermis and epidermal tongues (Supplemental Fig. 1B). Consistent with the literature [32], notable re-expression occurred in 7-day wounds. Again, absence or presence of physiological meprin expression did neither majorly influence distribution nor staining intensity of E-cadherin (Supplemental Fig. 1B).

We then asked if the slower re-epithelialization observed during combined meprin α and meprin β deficiency was due to other cell-intrinsic changes. Toward this end, we isolated keratinocytes from tail skin of adult WT, *Mep1a*^{-/-}, *Mep1b*^{-/-}, and *Mep1a*^{-/-}/*Mep1b*^{-/-} mice. The isolated primary keratinocytes were subsequently grown to confluent monolayers, which were scratch wounded. In this assay, keratinocytes of different genotypes did not significantly differ in their ability to close scratch wounds (Supplemental Fig. 2). However, keratinocytes lacking both meprins displayed, compared to WT keratinocytes, a mild tendency to faster healing (Supplemental Fig. 2).

Collectively, our results indicate that meprin-evoked autochthonous reduction in keratinocyte mobility is not responsible for the mild, protracted re-epithelialization of wounds lacking both meprins.

Combined meprin deficiency reduces macrophage abundance in wounds

Since meprins have been implicated as both positive and negative modulators of inflammation [27] we next investigated this. By flow cytometry we analyzed the abundance of neutrophils and macrophages in 3-day-old wounds from WT, *Mep1a*^{-/-}, *Mep1b*^{-/-}, and *Mep1a*^{-/-}/*Mep1b*^{-/-} mice. Neutrophils were most abundant but the meprin status did not affect their numbers (Fig. 3C). Contrastingly, in 3-day-old *Mep1b*^{-/-} wounds a tendency to decrease in macrophages was noted and *Mep1a*^{-/-}/*Mep1b*^{-/-} wounds contained significantly fewer macrophages compared

to their WT counterpart (Fig. 3C). Staining of wounds revealed evenly distribution of macrophages in the wound bed of 3-day-old wounds of all genotypes; however, fewer macrophages were clearly present in *Mep1b*^{-/-} and *Mep1a*^{-/-}/*Mep1b*^{-/-} wounds (Fig. 3D).

To find some indications to why inflammation was altered in double meprin deficient wounds we used a quantitative polymerase chain reaction (qPCR) array to screen for altered expression of inflammation-related factors. To reduce the complexity of the analyses, we employed only *Mep1a*^{-/-} and *Mep1b*^{-/-} wounds vis-à-vis WT wounds (Supplemental Fig. 3A and Supplemental Table 1). We looked for genes that showed similar tendencies to be increased or decreased in both *Mep1a*^{-/-} and *Mep1b*^{-/-}. Here, the IL-1 system stood out (Supplemental Fig. 3A). qPCR analyses of day 3 wounds revealed that expression of *Il1a* was significantly decreased in *Mep1b*^{-/-} and *Mep1a*^{-/-}/*Mep1b*^{-/-} compared to WT (Supplemental Fig. 3B). *Il1b* and *Il1rap* – the encoded protein IL-1 receptor accessory protein initiates signaling events after IL-1 ligands associate with their cognate receptor – were also significantly lower expressed in *Mep1b*^{-/-} wounds (Supplemental Fig. 3B).

Meprins are players in dermal healing

The earlier flattening of *Mep1a*^{-/-} deficient wounds suggested changes in dermal healing (Fig. 2D). Consequently, we analyzed granulation tissue formation and dermal healing. Staining of day 7 wounds rendered compared to WT relatively stronger staining intensity for α -smooth muscle actin (α SMA) positive myofibroblasts in *Mep1a*^{-/-} wounds, whereas this intensity was weaker for *Mep1b*^{-/-} and *Mep1a*^{-/-}/*Mep1b*^{-/-} wounds (Fig. 4A). Lower abundance of α SMA in *Mep1b*^{-/-} and *Mep1a*^{-/-}/*Mep1b*^{-/-} wounds was confirmed by western blotting (Supplemental Fig. 4A). Although the distribution of α SMA positive myofibroblasts was largely similar among the different genotypes, the altered α SMA abundance could indicate subtle differences in dermal healing.

Fibronectin is one of the first ECM proteins deposited in granulation tissue, and a substrate of both meprins [27,35]. In early granulation tissue it is a main transmitter of force, which promotes myofibroblast formation [36,37]. 7 days after wounding fibronectin was significantly reduced in *Mep1b*^{-/-} wounds compared to *Mep1a*^{-/-} or *Mep1a*^{-/-}/*Mep1b*^{-/-} wounds (Fig. 4A and Supplemental Fig. 4B). Although fibronectin was not reduced in *Mep1a*^{-/-}/*Mep1b*^{-/-} wounds, its deposition in granulation tissue appeared heterogeneous with thick fibronectin-rich structures mixed with areas devoid of fibronectin. After 14 days, *Mep1b*^{-/-} wounds compared to WT or *Mep1a*^{-/-} displayed normal fibronectin levels but significant increase

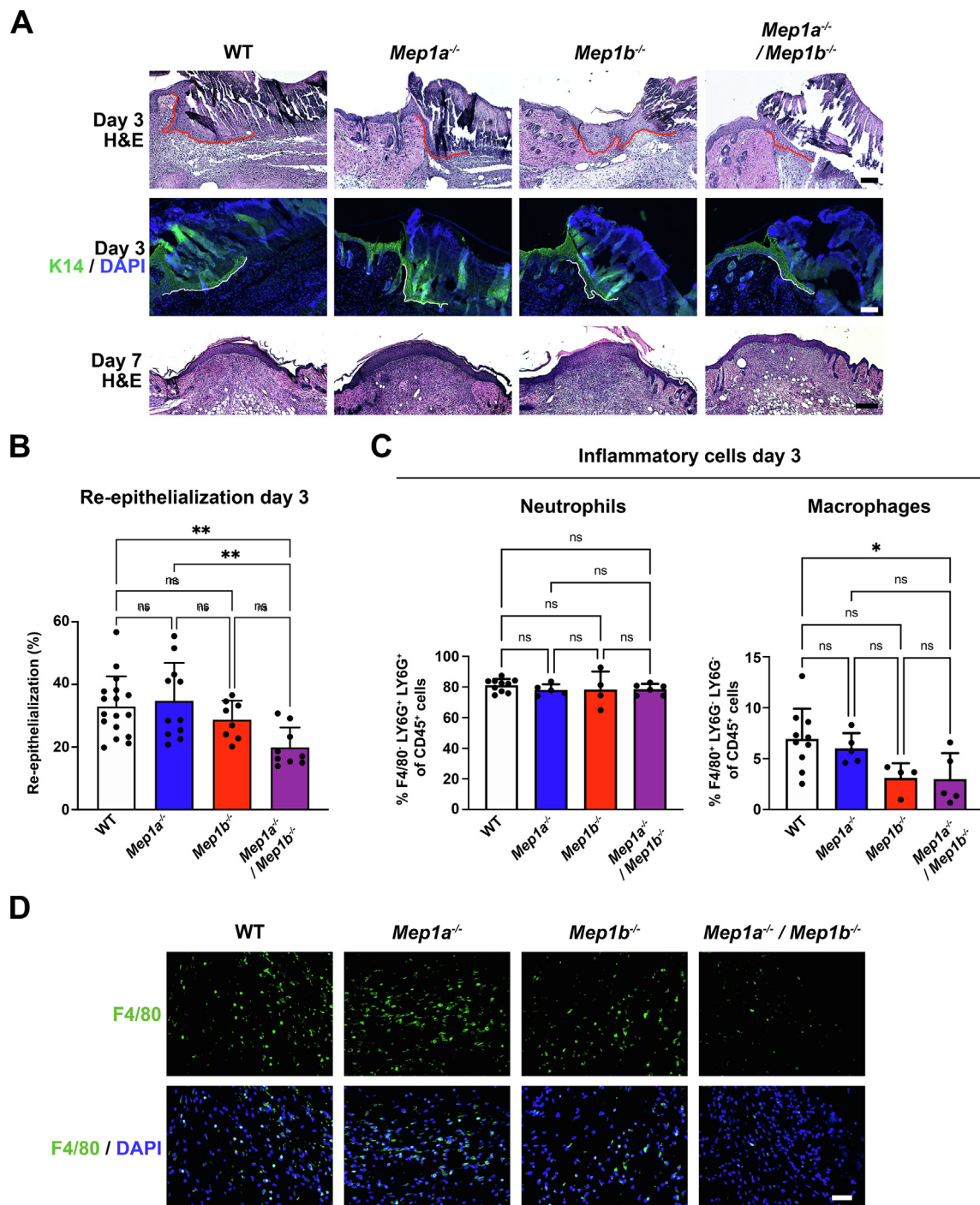


Fig. 3. Combined loss of meprins delays re-epithelialization. A, Hematoxylin & eosin (H&E) staining of sections from the middle of the wounds 3 or 7 days after wounding or keratin 14 (K14) staining to better visualize the epidermal tongue in 3-day-old wounds. White line indicates the epidermal tongue. Nuclei were counterstained with DAPI (blue). Scale bar = 50 μ m for the two top panels and = 100 μ m for the bottom panel. B, Bar graph showing quantification of percentage re-epithelialization of 3-day wounds as determined by histological measurements. Individual values for left and right wounds of the same animals ($n = 9-18$), mean \pm S.D. are shown, $**P < 0.01$ as analyzed by one-way ANOVA with Tukey's correction. C, Flow cytometry analysis for the abundance of neutrophils and macrophages in healthy 3-day wounds. Values for individual wounds ($n = 4-10$), mean \pm S.D. are shown, $*P < 0.05$ as analyzed by one-way ANOVA with Tukey's correction. D, Staining of 3-day wounds for the macrophage marker F4/80. Nuclei were counterstained with DAPI (blue). Scale bar = 50 μ m. (For interpretation of the references to colour in this figure legend, the reader is referred to the web version of this article.)

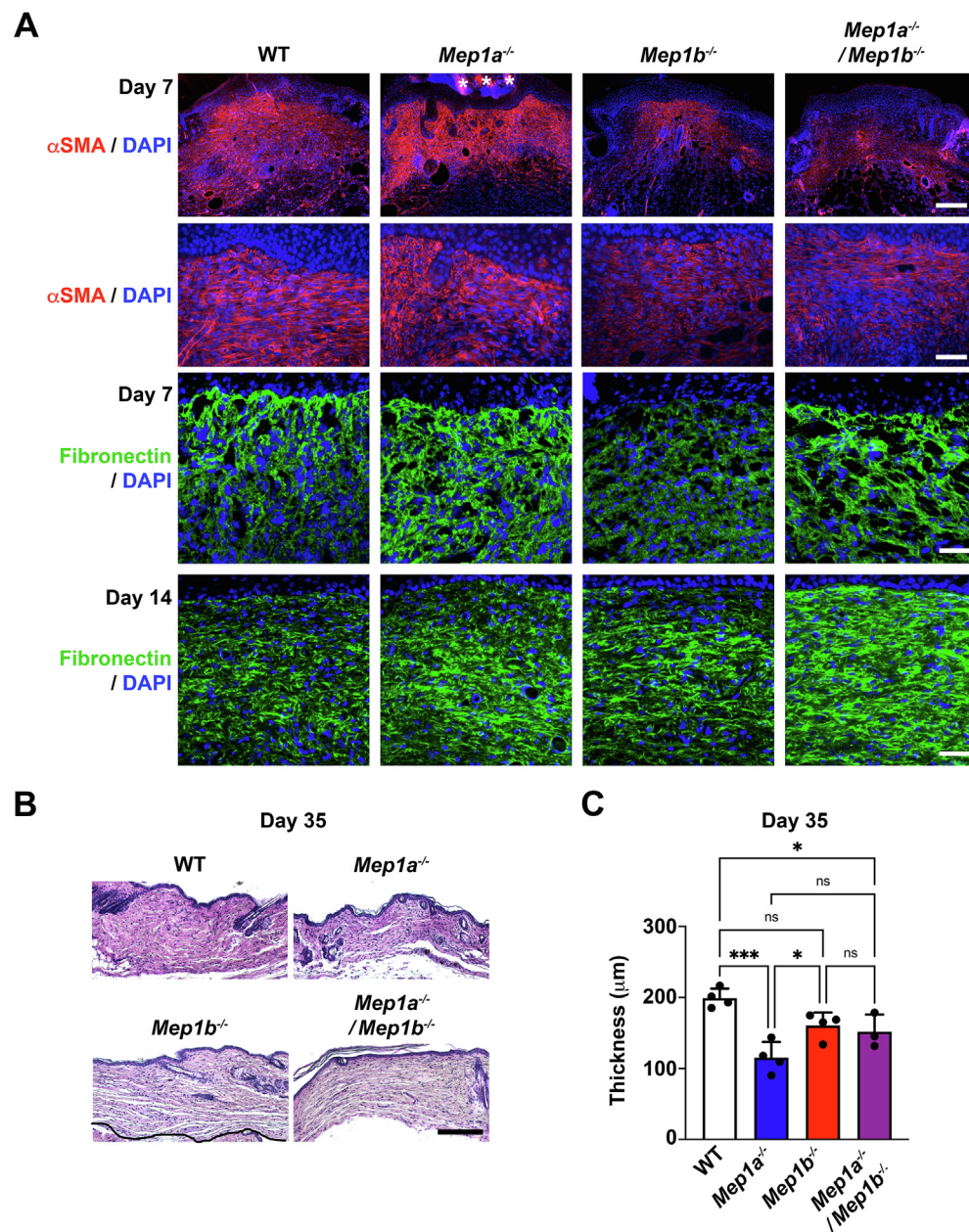


Fig. 4. Meprins are involved in granulation tissue formation and dermal healing. A, 7-day wounds stained for α -smooth actin (α SMA) (red) and 7- and 14-day wounds stained for fibronectin (green). Asterisks indicate non-specific staining of the scab. Nuclei were counterstained with DAPI (blue). Scale bar top panels for α SMA and fibronectin = 200 μ m, mid and bottom panels for α SMA and fibronectin = 50 μ m. B, Hematoxylin & eosin staining of sections from the middle of healing wounds 35 days after wounding. Scale bars = 200 μ m. C, Bar graph showing quantification of dermal thickness in 35-day wounds. N = 3–4 wounds per genotype, values represent mean \pm S.D. * P < 0.05; *** P < 0.001 as analyzed by one-way ANOVA with Tukey's correction. (For interpretation of the references to colour in this figure legend, the reader is referred to the web version of this article.)

was observed in combined meprin deficient wounds (Fig. 4A and Supplemental Fig. 4B).

35 days after wounding the healed dermis was thinner for all meprin deficient wounds compared to WT – a tendency for *Mep1b*^{-/-} and significant for *Mep1a*^{-/-} and *Mep1a*^{-/-}/*Mep1b*^{-/-} (Fig. 4B and C), with *Mep1a*^{-/-} having the thinnest dermis.

This observation prompted us to next investigate the appearance of the dermal collagen matrix. Day 35 wounds were analyzed by transmission electron microscopy. Lower magnifications indicated loose and patchy appearance of the dermal collagen matrix in single meprin deficient mice (Fig. 5A). Whereas, interestingly, in wounds

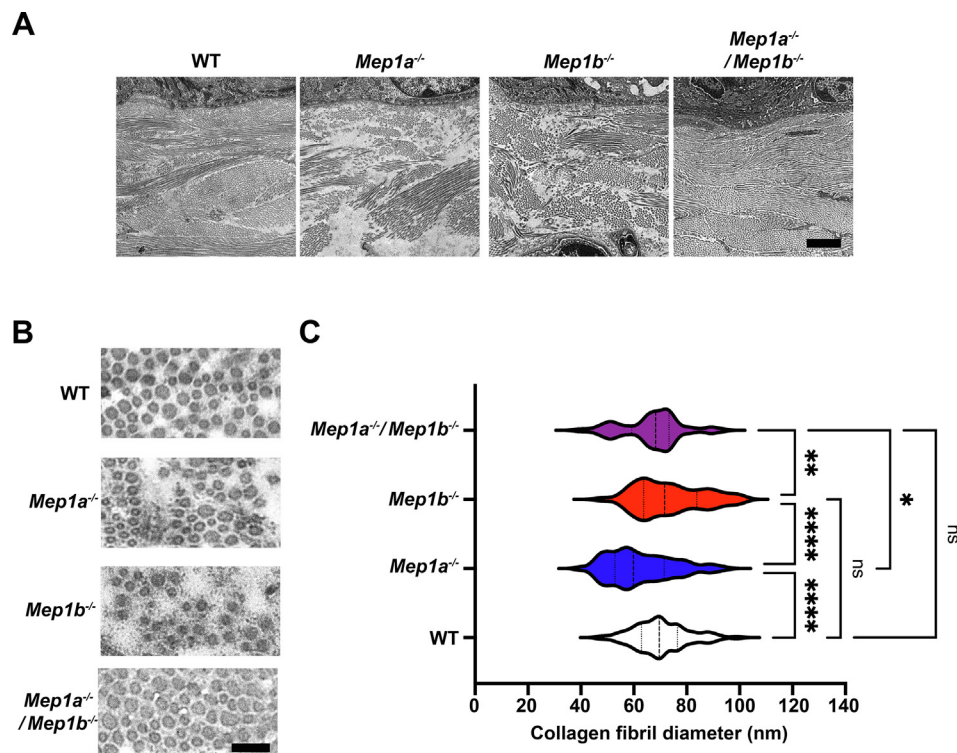


Fig. 5. Altered appearance of the dermal collagen matrix in healing single meprin deficient wounds. A, Low power transmission electron microscopy images of 35-day wounds. Note the looser and less connected arrangement of collagen bundles in single meprin deficient wounds. Scale bar = 500 nm. B, Higher power magnification of dermal collagen fibrils in wounds described in A. Scale bar = 100 nm. C, Graphs shows quantification of the diameter of dermal collagen fibrils in wounds described in A. Indicated in the graph are median, 25th and 75th percentiles. ** $P < 0.01$; *** $P < 0.001$; **** $P < 0.0001$ as analyzed by one-way ANOVA with Tukey's correction.

from combined meprin deficient mice it appeared as in WT (Fig. 5A). Quantification of individual collagen fibrils at higher magnification revealed significantly thinner fibrils in 35-day wound dermis of *Mep1a*^{-/-} mice (Fig. 5B and C). The diameter of collagen fibrils in wounds from combined meprin deficient mice was also significantly smaller than those of single *Mep1b*^{-/-} mice (Fig. 5B and C). Collectively, these data show that meprins are involved in dermal healing and regulate *de novo* collagen fibrillogenesis.

Meprin α is a physiological processor of pro-collagen VII

Studies of healing skin in mice with *Bmp1*/*mTld* and *Tll1* deficiency had revealed expected disturbance of maturation of many BTPs substrates including fibrillar collagens and laminin-332 [9]. However, despite the ability of BMP1 to mature collagen VII in vitro [8], pro-collagen VII to collagen VII conversion still occurs in BTP deficient mice [9]. This together with previous reports of retained collagen VII maturation in *Bmp1*/*mTld* deficient embryonic skin [8] and shared substrates between BTPs and meprins, prompted us to inves-

tigate potential meprin-mediated maturation of collagen VII.

First, recombinant human pro-collagen VII was incubated with or without human meprin α or meprin β at a ratio of 10:1 (40 nM:4 nM) for 2 h at 37 °C and analyzed by gel electrophoresis (Fig. 6A). This revealed that both meprin α and meprin β were able to convert pro-collagen VII to a slightly faster-migrating protein (Fig. 6A, left). Subsequently, meprin-digested collagen VII and undigested collagen VII were subjected to mass spectrometry analyses to identify cleavage sites. Focusing on C-terminal processing, LPSY_{2819/2820}AADTAGSQ was disclosed a potentially specific cleavage site of meprin α in the non-collagenous (NC) 2 domain. For meprin β two sites were identified in the NC2 domain, the same as for meprin α and in addition the site previously reported for BMP1 LPSYAA_{2821/2822}DTAGSQ [8] (Fig. 6A and Table S2). Additionally, in the NC2 domain of the meprin α -digested collagen VII, cleavage between R_{2927/2928}R was found (Table S2). However, these amino acids are outside the region identified through natural mutations to contain the site processed during collagen VII maturation [38]. Furthermore, the relatively low preference of meprin

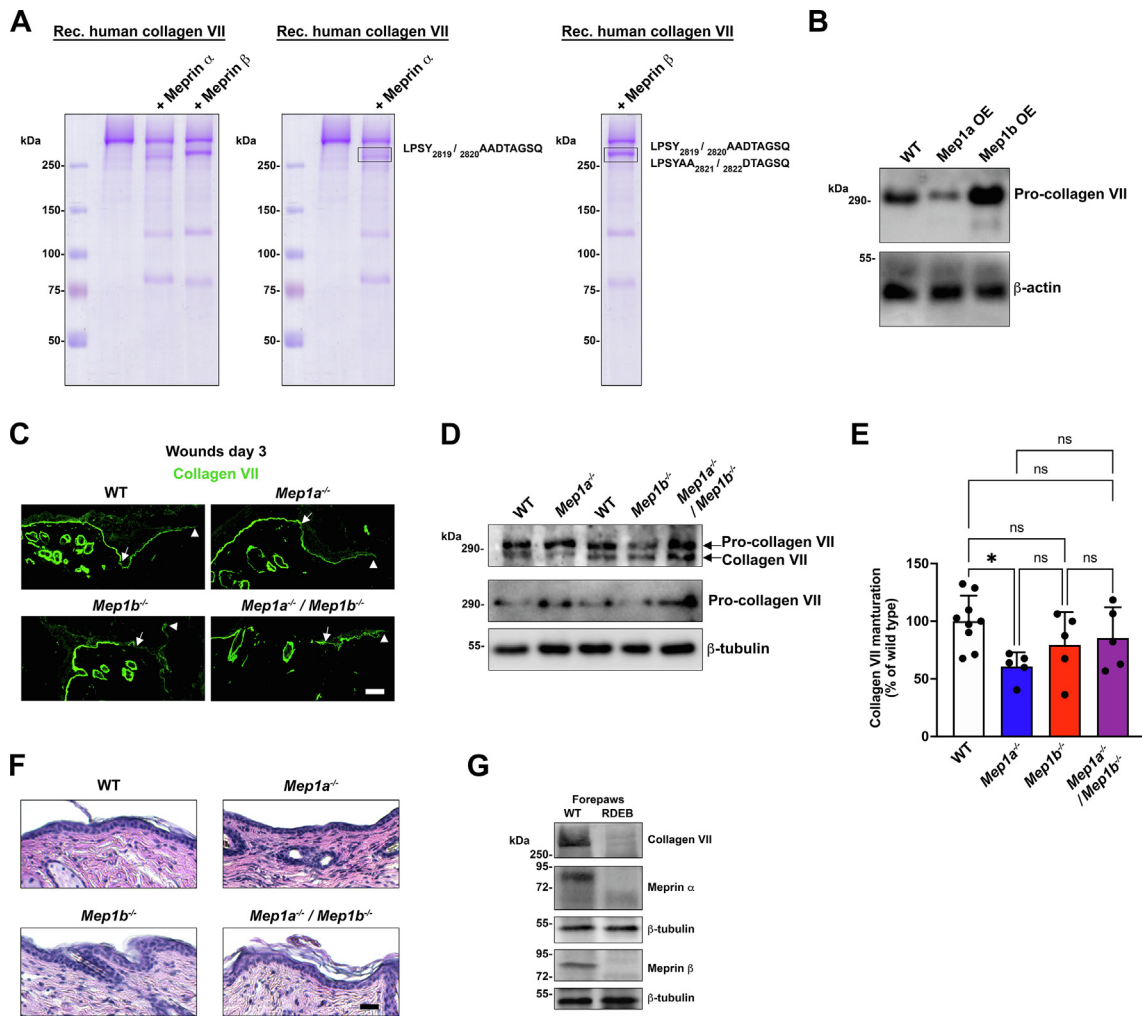


Fig. 6. Meprin α is a physiological maturing proteinase of pro-collagen VII. A, Coomassie-stained gels onto which human recombinant collagen VII $-/+$ prior incubation with meprin α and meprin β was loaded. The two right panels show the same gel as presented to the left but with the cleavage sites identified with mass spectrometry listed. B, Western blotting of fibroblast cell and matrix lysates from WT murine fibroblasts or murine fibroblasts over-expressing (OE) meprin α (Mep1a) and meprin β (Mep1b). The blots were probed with a collagen VII antibody only recognizing pro-collagen VII. β -Actin was used as loading control. C, Staining of 3-day wounds for collagen VII. The antibody is directed to the NC1 domain and detects both pro- and mature collagen VII. Arrowheads indicate deposition of collagen VII under the epidermal tongues. Scale bar = 50 μ m. D, Western blotting of lysates from 7-day-old wounds. The blots were probed with an antibody detecting both pro- and mature collagen VII or only pro-collagen VII. β -Tubulin was used as loading control. E, Quantification of the ratio of mature- vs. pro collagen VII detected by western blots as in D and expressed as the percentage found in WT wounds. Individual values from different mice ($n = 5-9$), mean \pm S. D. are shown, $*P < 0.05$ as analyzed by one-way ANOVA with Tukey's correction. F, Hematoxylin & eosin staining of sections from 14-day wounds. Scale bar = 50 μ m. G, Western blotting of protein lysates extracted from paw skin of mice with advanced RDEB or WT littermates. The blots were probed for meprin α and meprin β . β -Tubulin was used as loading control.

α for arginine in the P1' position calls for caution of the specificity of this cleavage [39]. It cannot be excluded that the detection was caused by back exchange of ^{18}O to ^{16}O after proteolysis.

To analyze collagen VII processing in a context in which competition from other potential meprin substrates occurred, we assessed pro-collagen VII to collagen VII conversion in murine fibroblasts overexpressing meprin α or meprin β . Western

blotting of fibroblast cell and matrix lysates with an antibody directed to the part of the NC2 domain that is removed during maturation of pro-collagen VII to collagen VII, indicated increased processing upon meprin α overexpression (Fig. 6B).

Next, we investigated collagen VII in murine WT and meprin-deleted skin wounds. In day 3 wounds of all genotypes, linear deposition of collagen VII below the epidermal tongues was seen (Fig. 6C).

Importantly; however, western blotting of protein lysates from 7-day wounds revealed significantly lower conversion of pro-collagen VII to mature collagen VII in meprin α deficient wounds (Fig. 6D and E). Slight but not significant tendencies to reduced processing of collagen VII in meprin β or combined meprin deficient wounds were also observed. Improved collagen VII processing in combined meprin deficient wounds compared to meprin α deficient wounds could indicate compensation by other proteinases. Indeed, increase of BTP and MMP gene expression occurs in single meprin deficient skin [20]. Analysis of *Bmp1/mTld* gene expression showed that in skin wounds there was a non-significant trend toward increase in *Bmp1/mTld* upon single meprin deletion (Supplemental Fig. 5). This was not observed in *Mep1a^{-/-}/Mep1b^{-/-}* skin wounds (Supplemental Fig. 5).

Clinical observations have shown that mutations leading to disruption of the NC2 domain cleavage site, and consequently inability to convert pro-collagen VII to collagen VII, impairs the formation of stable anchoring fibrils causing genetic skin fragility – recessive dystrophic epidermolysis bullosa (RDEB) [38]. Anchoring fibrils are extracellular suprastructures that attach the epidermal basement membrane to the underlying papillary ECM [40]. Histological assessment of healed wounds revealed no obvious epidermal-dermal separation – a histological hallmark of RDEB – in re-epithelialized 14-day single or combined meprin deficient wounds (Fig. 6F).

Meprins are reduced in RDEB skin

As introduced above, genetically evoked collagen VII deficiency causes RDEB. It progresses from skin blistering that occurs at the level below the epidermal basement membrane to dermal fibrosis [41]. Strategies to treat the disease include cellular therapies or protein-replacement therapies that supplement the skin with pro-collagen VII [42]. Since inability to mature collagen VII impairs the formation of functional anchoring fibrils [38], it may be important for maximal efficacy of such strategies that the capability to mature collagen VII is not altered in RDEB skin. Toward this end, we assessed meprin abundance in skin from mice with advanced RDEB. Interestingly, we noted compared to locoregional matched WT skin dramatic reduction in the abundance of both meprins in RDEB skin (Fig. 6G), which at least in part was caused by reduced gene expression (data not shown). Furthermore, previous mass spectrometry-based proteomics has revealed that the abundance of natural inhibitor of meprins but not BTPs – fetuin B [43] – is significantly increased in fibrotic RDEB mouse skin compared to WT mouse skin [44]. Collectively, this suggested reduced meprin activity in RDEB. Indeed, measurement of meprin β activity confirmed significant reduction of its activity in fore-

paw skin from RDEB mice with advanced fibrosis (Supplemental Fig. 6).

To gain insight whether the cause was cell intrinsic or microenvironmental we analyzed meprin α and meprin β abundance in cultured WT and RDEB keratinocytes and fibroblasts. Human donor-derived cells were used because of their phenotypic stability. Here, the RDEB donor-derived keratinocytes and fibroblasts showed similar meprin α and meprin β abundance as their WT counterparts (Supplemental Fig. 7), alluding to non-cell intrinsic cause of meprin deficiency.

Collectively, these observations suggest generalized impaired meprin activity in RDEB skin with advanced disease.

Discussion

Here, we show that meprins are dispensable in mice for macroscopic wound healing to progress in an appropriate timely manner. On more detailed levels; however, it is clear that meprins support the various parts of wound healing.

Combined meprin deficiency yielded transiently reduced re-epithelialization of wounds. Although we did not determine the mechanistic cause to the delayed re-epithelialization one influencing factor may be the reduced infiltration of macrophages in wounds [45]. Both meprins can activate pro-IL-1 β [27]. IL-1 cytokines, their receptors and regulators are heavily interconnected and co-regulation of gene expression occurs [46]. Expression of IL-1 cytokines is induced by inflammatory factors, including auto-induction [46]. Thus, changed gene expression levels could be a consequence of altered pro-cytokine activation. This could influence the inflammatory response and recruitment of immune cells after injury.

An interesting observation from our studies, which has also been made in previous investigations [47], is the unpredictable outcome of single vs. double meprin deficiency. Loss of both meprins in some cases, including dermal thickness and collagen fibrillogenesis, morphologically normalized abnormalities observed by single meprin deficiency. This highlights compensation and intricate connections within the proteinase web.

The purpose of this study was to gain insight into the role of meprins in dermal healing. On the one hand, potential pro-healing, pro-fibrotic actions would be suspected because both meprin α and meprin β had been reported to be elevated in keloid scars, as well as elevated in natural and experimentally-induced fibroproliferative conditions [48]. On the other hand, meprin α expression in the aforementioned conditions could potentially be tissue preservative, as meprin α could limit fibrosis through generation of the inflammation-reducing peptide Ac-SDKP from thymosin- β 4 [49] – an axis also active in skin [50]. Our data indicate that in the context of physiological wound healing meprin

α supports dermal healing by promoting dermal growth and formation of a collagen matrix.

Previous studies have shown that pro-collagen VII can be converted by BMP-1 to collagen VII [8,51]; however, *in vivo* collagen VII maturation still occurs in murine skin deficient of multiple BTPs [9]. To our knowledge, we show for the first time reduced collagen VII maturation *in vivo* in a proteinase deficient model. Meprin α appears to be the main meprin responsible for collagen VII maturation, which is reasonable, given its localization to basal keratinocytes and weak but noticeable abundance in homeostatic dermis, which is highly increased after injury.

It is important to say that meprin α alone is not solely responsible for collagen VII maturation in skin, as this still occurs when meprin α is absent, albeit at a lower level. Despite reduced collagen VII processing linear deposition of collagen VII was seen under epidermal tongues in healing meprin α -deleted wounds. This is in accordance with maturation of pro-collagen VII not being strictly needed for deposition at epidermal basement membrane zone, since linear deposition of maturation-deficient collagen VII occurs [38]. The absence of conspicuously impaired epidermal to dermal cohesion in healed wounds and skin lacking meprin α could be accounted for by that, as stated, collagen VII is still partially matured. However, it is possible that under conditions where the abundance of collagen VII is restricted this reduced processing of collagen VII could manifest in reduced strength of dermal-epidermal cohesion and skin blistering. Therefore, this may need to be considered when optimizing RDEB therapies, which are based on delivering pro-collagen VII to RDEB skin.

Collectively, our study shows that meprins fill minor but distinct and partially non-redundant functions during skin wound healing. Although lack of meprin-evoked activities were insufficient to cause a clinically notable wound healing impairment, it is possible that their dysregulation could act as confounding factors to wound healing pathologies. Future studies are needed to elucidate such possible links. Our findings underscore meprin activities in dermal ECM homeostasis.

Materials and methods

Ethics

The wound healing studies in WT and meprin deficient mice, and RDEB mouse breeding and sample collection were approved by the regional review board (Regierungspräsidium Freiburg, Freiburg, Germany; approval number G17-86, G14-93 and G15-140). Studies using human-derived material were approved by the ethics committee of the University of Freiburg (approval nos. 425/14 and 318/18).

Human cells

Human keratinocytes and fibroblasts were isolated from skin biopsies using routine protocols [52]. Briefly, after epidermal dermal separation with dispase, epidermal sheets were dissociated to single cells with trypsin and keratinocytes were then seeded on collagen-coated cell culture plates. Fibroblasts were isolated from outgrowths of explant cultures. The identity of keratinocytes and fibroblasts were confirmed by staining of keratinocyte and fibroblast-specific markers including keratin 14 and fibroblast activation protein, respectively. Human keratinocytes were cultured in Keratinocyte-SFM medium (Gibco), with addition of supplements according to the manufacturer's instruction and 0.2% Pen/Strep (Gibco). Fibroblasts were cultured in Dulbecco's modified Eagle's medium (DMEM) (Gibco) containing 4.5 g/L glucose, 10% fetal bovine serum (FBS) (Sigma Aldrich), 1% Pen/Strep (Gibco) and 1% L-Glutamine (Gibco). Cells from donors with RDEB were selected based on absence of collagen VII in western blotting analyses.

Murine cells

Fibroblasts were isolated from newborn murine skin of WT or meprin deficient mice by separation of the epidermis and dermis through incubation in dispase (2.5 U/ml), followed by digestion of the dermis with collagenase type I (1 U/ml) (Serva). Murine primary fibroblasts from skin were cultured in DMEM/F-12 medium (Gibco) with 10% FBS (Sigma Aldrich), 1% Pen/Strep (Gibco) and 1% L-Glutamine (Gibco). Keratinocytes were isolated from adult tails by incubating tail skin with 1% trypsin/DMEM for 1 h at 37 °C following physical separation of the epidermal and dermal sheets. The epidermal sheet was grinded through a 40 μ m cell strainer and cells seeded on collagen I-coated dishes. Murine keratinocytes were cultured in CnT-57 medium (CellnTec).

Wound healing experiments

All mice were on the C57BL/6 background and the generation of the mice has previously been described [47,53–55]. *Mep1b*^{-/-} were bred as homozygous, and due to the lower fertility *Mep1a*^{-/-} mice were generated from heterozygote mice. WT mice from these breedings were used as control for all experiments. All mice were kept in special-pathogen-free animal facilities and provided food and water *ad libitum*. The mice were bred in an animal facility at the University of Kiel before shipping to an animal facility at University of Freiburg for the analyses. Before the experiment the mice were given one week to acclimatize. The study was designed to comply with the ARRIVA guidelines [56]. The sample size was calculated on the variance from previous studies [57] by performing

a Log-Rank test with a power of 80% and for a P value $<5\%$.

Back skin of 7-week-old mice were and punched through a fold with a 6 mm punch biopsy tool to create two full-thickness wounds on the mid back as previously described [58]. Photos were taken immediately after wounding and then every-other day until the wounds had closed. For each photo a sticky ruler was placed next to the wound as a size reference. Selected mice per group, 4–8 mice per timepoint, were sacrificed at 3, 7, 14, 21 and 35 days after wounding for genetic, histological and biochemical analyses. In total 132 mice were used.

Macroscopic wound healing was calculated from photographs by measuring the wound size with Image J (NIH) and expressed as the percentage of the size of the wound directly after wounding, which was set to 100%.

Histological analyses

Wounds were harvested using an 8 mm punch biopsy tool and immediately fixed in formalin for at least 12 h. The wounds were dehydrated and paraffin embedded, sectioned, rehydrated, stained with hematoxylin and eosin and dehydrated before mounting. The stained sections were analyzed and photographed using an Axioplan 2 fluorescence microscope (Zeiss) and a monochrome Axiocam camera (Zeiss). For examination of wound re-epithelialization, sequential sections spanning the middle of the wound were analyzed to find the largest gap. Two sections per wound and both wounds per mouse were analyzed. Using Image J the total wound length and the length of the epidermal tongues were measured. The mean value per wound was plotted. Re-epithelialization was expressed as the percentage of wound covered by new epithelium as previously described [59].

Immunofluorescence staining

Tissue, either embedded in optimal cutting temperature medium (OCT) (Sakura) and snap frozen or paraffin-embedded, was sectioned and stained. Before staining frozen sections were fixed in ice-cold acetone for 5 min, for sections of paraffin-embedded material heat-mediated antigen retrieval with sodium citrate buffer was performed.

Sections were blocked with 4% bovine serum albumin (BSA) in phosphate-buffered saline (PBS) or tris-buffered saline (TBS) for 30 min at room temperature before staining with primary antibodies at 4 °C overnight. Sections were washed in PBS or TBS with 0.05% Tween-20 and stained with fluorophore-coupled secondary antibodies. Cell nuclei were counterstained with 4',6-diamidino-2-phenylindole (DAPI).

The stained sections were analyzed with an Axioplan 2 fluorescence microscope and a

monochrome Axiocam camera. For comparative analyses images were captured at one session with identical settings and exposure time.

Western blotting

Tissue lysates were prepared as previously described [60] by crushing deep-frozen tissue with a hammer on metal plates placed on dry ice. The crushed tissue was boiled in 6X blue sample buffer with 8 M urea. After centrifugation, dilution in TBS and re-boiling the samples were loaded onto SDS-PAGEs and western blotting performed under standard conditions. For western blotting either PVDF or nitrocellulose membranes were used.

For analyses of RDEB model mice, collagen VII hypomorphic mice were used [61]. Protein lysates were prepared as described above from heavily fibrotic forepaws of 12-week-old mice.

Antibodies

The following antibodies were used: Rabbit anti-meprin α , rabbit-meprin β (both in house, University of Kiel), rat anti-meprin β (MAB28951, R&D systems), mouse anti- α SMA-Cy3 conjugated (clone 1A4, Sigma-Aldrich), mouse anti-keratin-14 (ab7800, Abcam), rabbit anti-involucrin (ab28057, Abcam), rabbit anti-loricrin (ab24722, Abcam), mouse anti-E-cadherin (BD610181, BD Biosciences), rabbit anti-fibronectin (ab2413, Abcam), rat anti-F4-80 (Clone MA1, Roche), rabbit anti-mouse collagen VII NC1 domain [62], and a rabbit anti-mouse collagen VII NC2 domain (pro-collagen VII antibody).

Antibodies for flow cytometry analysis were: anti-CD45 APC/Cy7 (clone 30-F11, BioLegend), anti-CD11b (clone M1/70, BDHorizon), anti-F4/80 PerCP/Cy5.5 (clone BM8, BioLegend), anti-mouse Ly6G Pe/Cy7 (clone 1A8, BioLegend) anti-Ly6C PeLy7 (clone 1 HK1.4, BioLegend).

The pro-collagen VII antibody was generated based on amplified cDNA from murine WT skin comprising the nucleotides encoding from amino acid H-2820 to A-2944. A C-terminal GST fusion protein was created by inserting the PCR product in the PGEX6P1 plasmid (Thermo Fisher Scientific). Protein was expressed in BL21-DE3 E. coli to allow high level of protein expression. Antibodies were raised in rabbits by injecting of the purified 200 μ g NC2-GST fusion peptide (Eurogentec). Specificity of the antibodies was examined by western blotting of skin lysates from WT and RDEB model mice.

Analysis of meprin processing of collagen VII

Recombinant collagen VII was purified from HEK-293 cells as previously described [63]. 40 nM recombinant collagen VII was incubated with 4 nM meprin α or meprin β for 2 h at 37 °C. After separation on SDS-PAGEs and staining with coomassie

blue the bands corresponding to full-length and processed collagen VII were cut out and subjected to mass spectrometry-based analysis as previously described [20]. Briefly bands for the C-terminal analysis were dehydrated with acetonitrile. Five μ l trypsin (5 ng/ μ l in 50% $H_2^{18}O$ /10 mM ammonium bicarbonate) was added and the gel bands were allowed to rehydrate and digested over night at 37 °C. Peptides were extracted by sonication and subjected to LC–MS/MS analysis using a Dionex U3000 nanoUHPLC coupled to a Q Exactive Plus mass spectrometer (both from Thermo Scientific). The acquired MS/MS-spectra were searched with the SequestHT and Mascot algorithm against the entire reviewed database of *homo sapiens* with common contaminants (cRAP, <http://www.thegpm.org/crap/>) appended to the database (20,380 sequences). A MS mass tolerance of 10 ppm and a MS/MS tolerance of 0.02 Da was used. Peptide grouping was applied to group Peptide Spectral Matches (PSMs) with the same modification under the same peptide. The protein group identifications were further filtered based on the following criteria: Proteins must be identified with at least two peptides of a false-discovery rate confidence ≤ 0.01 . C-terminal peptides are identified by the absence of an ^{18}O - isotope at the C-terminal α -carboxyl group.

Electron microscopy

For analysis of collagen fibril diameter and organization by electron microscopy, samples were cut into 5 × 5 mm pieces and submerged in 3% Glutaraldehyde in 0.1 M phosphate buffer (pH 7.4). The phosphate buffer contained 0.1 M KH_2PO_4 and 0.1 M $Na_2HPO_4 \cdot 2H_2O$ in a proportion of 4:21. They were then washed 0.1 mol/l cacodylate buffer and incubated in 1% osmium tetroxide solution. Samples were dehydrated in ethanol (25, 50, 75, 90, 100%) and propylene oxide, and embedded in an epoxy resin. Ultrathin (50 nm) sections (Ultracut S microtome; Leica Microsystems) were visualized using a Tecnai12 electron microscope operating a LaB6 electron source (FEI). Feret's diameter of dermal collagen fibrils was measured using Image J.

Flow cytometry analysis

Skin samples or full thickness wounds were collected in 1 ml PBS and placed on ice. Next, they were transferred into FACS-tubes and cut into small pieces with a pair of scissors. After this 500 μ l of LiberaseTM (Roche) were added and incubated for 1 h at 37 °C. Following digestion the solution was passed through a 40 μ m strainer and washed with 10 ml PBS and cells pelleted by centrifugation. The cell pellet was re-suspended in 100 μ l of PBS with 3% FBS and all samples were transferred into the wells of a 96-well plate. After pooling parts of all samples from 1 to 3 wells the

plate was centrifuged at 300×g for 3 min and the supernatant was discarded again. Next, the pellets were dissolved and blocked for 10 min in 10 μ l Mouse BD Fc BlockTM (BD Bioscience) at 4 °C. Cells were stained with the indicated directly-conjugated antibodies at 4 °C run on a BD FACSCantoTM II cytometer. Data were acquired with the DIVA software and analyzed by FlowJo.

Real-time qPCR analyses and inflammatory gene array

Cells or 30 μ g of tissue was collected and crushed while frozen, using mechanical force, until it had a homogeneous appearance. Afterwards, RNA was extracted using the RNeasy® Fibrous Tissue Mini Kit (Thermo Scientific) following the manufacturer's instructions. RNA was diluted in 40 μ l RNA-free water and stored at –80 °C for further steps. RNA was reverse transcribed with First strand cDNA Synthesis Kit K1612 (Thermo Scientific) and used for either real-time qPCR analyses or the inflammatory gene array.

qPCR analyses were performed using SYBR green (Bio-Rad) and a CFX96 Real Time system (Bio-Rad). The following primers were used: *Bmp1* forward CGCCTGTGCTGGTATGACTAT, reverse CACATCGCCACCGCCAAATG; *Tll1* forward GGTTGGTGGTCTCGGGTATTG, reverse TAGGCTCCGTTTTGTCTCTT; *Tll2* forward CCCCTTGCGACCACTCTTG, reverse CCAGAGC AATATCTCCCA-GAA; *Mep1a* forward AATG CTTTGGATACAACCTGCG, reverse TCCATC TGCTT GAGGGATCTC; *Mep1b* forward GGA TTCTGGCATGAGCAGTCA, reverse TGGAAA GCGGTTTTACTGTAGTG; *Il1a* forward TCTC AGATTCACAAC TGTTTCGTG, reverse AGA AAATGAGGTCCGGTCTCACTA; *Il1b* forward GAA ATGCCACCTTTTGACAGTG, reverse TGGATG CTCTCATCAG-GACAG; *Il1rap* forward GGAAC TGGTTATTCCCTGCAA, reverse GCTCGGTG CATCCATTACCTT; *Gapdh* forward TTGATGG CAACAATCTCCAC, *Gapdh* reverse: CGTCCC GTAGACAAAATGGT; *BMP1* forward GGGTC ATC CCCTTTGTCATTG, reverse GCAAGGT CGATAGGTGAACACA; *mTLD* forward GTTC TGAGA-AGCCCGAGGTC, reverse GCACTCA TAACTGCCGAACG; *TLL1* forward TTGTTTTT TACGGGGAGCTATGG, reverse ATATCG CCCC AAATACAGCG; *TLL2* forward GCCAT GTGGTTGGGTTTTGG, reverse TGTC AA AGTCGTATG TCTCTCCC; *MEP1A* forward GCT TGGACCTC TTCAAGGGG, reverse GACG GAACATCTCAAAGGCAT; *MEP1B* forward GCTA AGGGAGTTA TCCTCAATGC, reverse CCCAAC CCGCCTATTTCTAC, *GAPDH* forward CCCATC ACCATCTTCCAG; *GAPDHR* reverse ATGAC CTTGCCACAGCC.

To gain an overview of inflammation-related changes in wounds of meprin knock-out mice cDNA from 3-day-old wounds of WT, meprin α and meprin β deficient mice was analyzed by a

RT2 Profiler™ PCR Array Mouse Inflammatory Response & Autoimmunity, Qiagen, Cat. No.: PAMM-077ZD. The arrays were run and analyzed following the manufacturer's on a CFX96 Real Time system.

Received 12 March 2021;

Accepted 3 May 2021;

Available online 13 May 2021

Enzymatic activity assay

Protein lysates of WT and RDEB paws were generated by grinding paws in a liquid nitrogen-cooled mortar and incubation of the grinded tissue in lysate buffer containing 1% triton x-100 and cOmplete® protease inhibitor cocktail without EDTA (Roche) for 8 h at 4 °C with mild shaking. Meprin β activity was measured in 200 μ g protein lysate using a specific meprin β fluorogenic peptide substrate (mca-EDEDED-dnp; Genosphere Biotechnologies) in final concentration of 50 μ M. The peptide consisted of a fluorophore (mca), a specific substrate peptide for meprin β (EDEDED), and a quencher (dnp). Fluorescence intensity was detected at 37 °C every 30 s for 120 min using a spectrophotometer (Tecan, Männedorf, Switzerland). For data analysis, slope of equal linear activity range of duplicates was compared between individual animals.

Statistical analysis

The GraphPad Prism 9 software was used for statistical analysis. The datasets were tested for normality and equal variance using Shapiro-Wilk and F tests. Statistical analyses were performed using one-way ANOVA with Tukey's correction, two-way ANOVA with Bonferroni correction or unpaired two-tailed Student's *t*-test. For all analyses, $P < 0.05$ was considered statistically significant.

Conflict of interest

The authors state that no conflict of interest exists.

Acknowledgements

We thank Dr. Somasundaram Prasath and Dr. Andreas Tholey Institute of Experimental Medicine, Christian-Albrechts-University Kiel, Germany for performing mass spectrometry analyses, which were supported by the Z2-project in CRC877 and Dr. Pauline Nauroy. Department of Dermatology, Medical Center – University of Freiburg for comments and suggestions on the manuscript. This work was supported by the German Research Foundation (DFG) through NY90/2-1 (AN), NY90/5-1 (AN), CRC850 project B11 (AN), CRC877 project A9 (CBP), and BE 4086/5-1 (CBP).

Appendix A. Supplementary data

Supplementary data to this article can be found online at <https://doi.org/10.1016/j.mbplus.2021.100065>.

Keywords:

Wound healing;
Extracellular matrix;
Fibrosis;
Inflammation;
Dystrophic epidermolysis bullosa

1 These authors contributed equally to this work.

Abbreviations:

ALP, astacin-like proteinase; BSA, bovine serum albumine; BTP, BMP-1/tolloid-like proteinase; DAPI, 4',6-diamidino-2-phenylindole; DEJ, dermal epidermal junction; DMEM, Dulbecco's modified Eagle's medium; ECM, extracellular matrix; FA, formic acid; FBS, fetal bovine serum; NC, non-collagenous; PBS, phosphate-buffered saline; qPCR, quantitative polymerase chain reaction; TBS, tris-buffered saline; WT, wild type; α SMA, α -smooth muscle actin

References

- [1]. Zigrino, P., Brinckmann, J., Niehoff, A., Lu, Y., Giebeler, N., Eckes, B., Kadler, K.E., Mauch, C., (2016). Fibroblast-derived MMP-14 regulates collagen homeostasis in adult skin. *J. Invest. Dermatol.*, **136**, 1575–1583. <https://doi.org/10.1016/j.jid.2016.03.036>.
- [2]. Nauroy, P., Nyström, A., (2020). Kallikreins: essential epidermal messengers for regulation of the skin microenvironment during homeostasis, repair and disease. *Matrix Biol. Plus.*, **6–7**, 100019. <https://doi.org/10.1016/j.mbplus.2019.100019>.
- [3]. Zhang, S., Duan, E., (2018). Fighting against skin aging: the way from bench to bedside. *Cell Transplant.*, **27**, 729–738. <https://doi.org/10.1177/0963689717725755>.
- [4]. Xue, M., Jackson, C.J., (2015). Extracellular matrix reorganization during wound healing and its impact on abnormal scarring. *Adv. Wound Care*, **4**, 119–136. <https://doi.org/10.1089/wound.2013.0485>.
- [5]. Eming, S.A., Martin, P., Tomic-Canic, M., (2014). Wound repair and regeneration: mechanisms, signaling, and translation. *Sci. Transl. Med.*, **6**, 265sr6. <https://doi.org/10.1126/scitranslmed.3009337>.
- [6]. Becker-Pauly, C., Höwel, M., Walker, T., Vlad, A., Aufenvenne, K., Oji, V., Lottaz, D., Sterchi, E.E., Debela, M., Magdolen, V., Traupe, H., Stöcker, W., (2007). The alpha and beta subunits of the metalloprotease meprin are expressed in separate layers of human epidermis, revealing different functions in keratinocyte proliferation and differentiation. *J. Invest. Dermatol.*, **127**, 1115–1125. <https://doi.org/10.1038/sj.jid.5700675>.
- [7]. Kronenberg, D., Bruns, B.C., Moali, C., Vadon-Le Goff, S., Sterchi, E.E., Traupe, H., Böhm, M., Hulmes, D.J.S., Stöcker, W., Becker-Pauly, C., (2010). Processing of procollagen III by meprins: new players in extracellular matrix assembly?. *J. Invest. Dermatol.*, **130**, 2727–2735. <https://doi.org/10.1038/jid.2010.202>.

- [8]. Rattenholl, A., Pappano, W.N., Koch, M., Keene, D.R., Kadler, K.E., Sasaki, T., Timpl, R., Burgeson, R.E., Greenspan, D.S., Bruckner-Tuderman, L., (2002). Proteinases of the bone morphogenetic protein-1 family convert procollagen VII to mature anchoring fibril collagen. *J. Biol. Chem.*, **277**, 26372–26378. <https://doi.org/10.1074/jbc.M203247200>.
- [9]. Muir, A.M., Massoudi, D., Nguyen, N., Keene, D.R., Lee, S.-J., Birk, D.E., Davidson, J.M., Marinkovich, M.P., Greenspan, D.S., (2016). BMP1-like proteinases are essential to the structure and wound healing of skin. *Matrix Biol. J. Int. Soc. Matrix Biol.*, **56**, 114–131. <https://doi.org/10.1016/j.matbio.2016.06.004>.
- [10]. Ge, G., Greenspan, D.S., (2006). BMP1 controls TGF β 1 activation via cleavage of latent TGF β -binding protein. *J. Cell Biol.*, **175**, 111–120. <https://doi.org/10.1083/jcb.200606058>.
- [11]. Anastasi, C., Rousselle, P., Talantikite, M., Tessier, A., Cluzel, C., Bachmann, A., Mariano, N., Dussoyer, M., Alcaraz, L.B., Fortin, L., Aubert, A., Delolme, F., El Kholiti, N., Armengaud, J., Fournié, P., Auxenfans, C., Valcourt, U., Goff, S.V.-L., Moali, C., (2020). BMP-1 disrupts cell adhesion and enhances TGF- β activation through cleavage of the matricellular protein thrombospondin-1. *Sci. Signal.*, **13** <https://doi.org/10.1126/scisignal.aba3880>.
- [12]. Kessler, E., Fichard, A., Chanut-Delalande, H., Brusel, M., Ruggiero, F., (2001). Bone morphogenetic protein-1 (BMP-1) mediates C-terminal processing of procollagen V homotrimer. *J. Biol. Chem.*, **276**, 27051–27057. <https://doi.org/10.1074/jbc.M102921200>.
- [13]. Imamura, Y., Steiglit, B.M., Greenspan, D.S., (1998). Bone morphogenetic protein-1 processes the NH₂-terminal propeptide, and a furin-like proprotein convertase processes the COOH-terminal propeptide of pro- α 1(V) collagen. *J. Biol. Chem.*, **273**, 27511–27517. <https://doi.org/10.1074/jbc.273.42.27511>.
- [14]. Ge, G., Seo, N.-S., Liang, X., Hopkins, D.R., Höök, M., Greenspan, D.S., (2004). Bone morphogenetic protein-1/tolloid-related metalloproteinases process osteoglycin and enhance its ability to regulate collagen fibrillogenesis. *J. Biol. Chem.*, **279**, 41626–41633. <https://doi.org/10.1074/jbc.M406630200>.
- [15]. Uzel, M.I., Scott, I.C., Babakhanlou-Chase, H., Palamakumbura, A.H., Pappano, W.N., Hong, H.H., Greenspan, D.S., Trackman, P.C., (2001). Multiple bone morphogenetic protein 1-related mammalian metalloproteinases process pro-lysyl oxidase at the correct physiological site and control lysyl oxidase activation in mouse embryo fibroblast cultures. *J. Biol. Chem.*, **276**, 22537–22543. <https://doi.org/10.1074/jbc.M102352200>.
- [16]. Amano, S., Scott, I.C., Takahara, K., Koch, M., Champlaud, M.-F., Gerecke, D.R., Keene, D.R., Hudson, D.L., Nishiyama, T., Lee, S., Greenspan, D.S., Burgeson, R.E., (2000). Bone morphogenetic protein 1 is an extracellular processing enzyme of the laminin 5 γ 2 chain. *J. Biol. Chem.*, **275**, 22728–22735. <https://doi.org/10.1074/jbc.M002345200>.
- [17]. Nyström, A., Bornert, O., Köhl, T., (2017). Cell therapy for basement membrane-linked diseases. *Matrix Biol. J. Int. Soc. Matrix Biol.*, **57–58**, 124–139. <https://doi.org/10.1016/j.matbio.2016.07.012>.
- [18]. Takahara, K., Lyons, G.E., Greenspan, D.S., (1994). Bone morphogenetic protein-1 and a mammalian tolloid homologue (mTld) are encoded by alternatively spliced transcripts which are differentially expressed in some tissues. *J. Biol. Chem.*, **269**, 32572–32578. [https://doi.org/10.1016/S0021-9258\(18\)31672-7](https://doi.org/10.1016/S0021-9258(18)31672-7).
- [19]. Jefferson, T., auf dem Keller, U., Bellac, C., Metz, V.V., Broder, C., Hedrich, J., Ohler, A., Maier, W., Magdolen, V., Sterchi, E., Bond, J.S., Jayakumar, A., Traupe, H., Chalaris, A., Rose-John, S., Pietrzik, C.U., Postina, R., Overall, C.M., Becker-Pauly, C., (2013). The substrate degradome of meprin metalloproteinases reveals an unexpected proteolytic link between meprin β and ADAM10. *Cell. Mol. Life Sci.*, **70**, 309–333. <https://doi.org/10.1007/s00018-012-1106-2>.
- [20]. Broder, C., Arnold, P., Vadon-Le Goff, S., Konerding, M. A., Bahr, K., Müller, S., Overall, C.M., Bond, J.S., Koudelka, T., Tholey, A., Hulmes, D.J.S., Moali, C., Becker-Pauly, C., (2013). Metalloproteinases meprin α and meprin β are C- and N-procollagen proteinases important for collagen assembly and tensile strength. *Proc. Natl. Acad. Sci. U.S.A.*, **110**, 14219–14224. <https://doi.org/10.1073/pnas.1305464110>.
- [21]. Becker-Pauly, C., Barré, O., Schilling, O., Auf Dem Keller, U., Ohler, A., Broder, C., Schütte, A., Kappelhoff, R., Stöcker, W., Overall, C.M., (2011). Proteomic analyses reveal an acidic prime side specificity for the astacin metalloproteinase family reflected by physiological substrates. *Mol. Cell. Proteomics*, **10** <https://doi.org/10.1074/mcp.M111.009233>.
- [22]. Prox, J., Arnold, P., Becker-Pauly, C., (2015). Meprin α and meprin β : procollagen proteinases in health and disease. *Matrix Biol.*, **44–46**, 7–13. <https://doi.org/10.1016/j.matbio.2015.01.010>.
- [23]. Tang, J., Bond, J.S., (1998). Maturation of secreted meprin α during biosynthesis: role of the furin site and identification of the COOH-terminal amino acids of the mouse kidney metalloproteinase subunit. *Arch. Biochem. Biophys.*, **349**, 192–200. <https://doi.org/10.1006/abbi.1997.0453>.
- [24]. Herzog, C., Haun, R.S., Ludwig, A., Shah, S.V., Kaushal, G.P., (2014). ADAM10 is the major sheddase responsible for the release of membrane-associated meprin A. *J. Biol. Chem.*, **289**, 13308–13322. <https://doi.org/10.1074/jbc.M114.559088>.
- [25]. Wichert, R., Scharfenberg, F., Colmorgen, C., Koudelka, T., Schwarz, J., Wetzel, S., Potempa, B., Potempa, J., Bartsch, J.W., Sagi, I., Tholey, A., Saffig, P., Rose-John, S., Becker-Pauly, C., (2019). Meprin β induces activities of A disintegrin and metalloproteinases 9, 10, and 17 by specific prodomain cleavage, FASEB. *J. Off. Publ. Fed. Am. Soc. Exp. Biol.*, **33**, 11925–11940. <https://doi.org/10.1096/fj.201801371R>.
- [26]. Peters, F., Scharfenberg, F., Colmorgen, C., Armbrust, F., Wichert, R., Arnold, P., Potempa, B., Potempa, J., Pietrzik, C.U., Häslér, R., Rosenstiel, P., Becker-Pauly, C., (2019). Tethering soluble meprin α in an enzyme complex to the cell surface affects IBD-associated genes, FASEB. *J. Off. Publ. Fed. Am. Soc. Exp. Biol.*, **33**, 7490–7504. <https://doi.org/10.1096/fj.201802391R>.
- [27]. Herzog, C., Haun, R.S., Kaushal, G.P., (2019). Role of meprin metalloproteinases in cytokine processing and inflammation. *Cytokine*, **114**, 18–25. <https://doi.org/10.1016/j.cyto.2018.11.032>.
- [28]. Arnold, P., Boll, I., Rothaug, M., Schumacher, N., Schmidt, F., Wichert, R., Schneppenheim, J., Lokau, J., Pickhinke,

- U., Koudelka, T., Tholey, A., Rabe, B., Scheller, J., Lucius, R., Garbers, C., Rose-John, S., Becker-Pauly, C., (2017). Meprin metalloproteases generate biologically active soluble interleukin-6 receptor to induce trans-signaling. *Sci. Rep.*, **7**, 44053. <https://doi.org/10.1038/srep44053>.
- [29]. Sammel, M., Peters, F., Lokau, J., Scharfenberg, F., Werny, L., Linder, S., Garbers, C., Rose-John, S., Becker-Pauly, C., (2019). Differences in shedding of the interleukin-11 receptor by the proteases ADAM9, ADAM10, ADAM17, meprin α , meprin β and MT1-MMP. *Int. J. Mol. Sci.*, **20** <https://doi.org/10.3390/ijms20153677>.
- [30]. Keiffer, T.R., Bond, J.S., (2014). Meprin metalloproteases inactivate interleukin 6. *J. Biol. Chem.*, **289**, 7580–7588. <https://doi.org/10.1074/jbc.M113.546309>.
- [31]. Uhlen, M., Fagerberg, L., Hallstrom, B.M., Lindskog, C., Oksvold, P., Mardingoglu, A., Sivertsson, A., Kampf, C., Sjostedt, E., Asplund, A., Olsson, I., Edlund, K., Lundberg, E., Navani, S., Szigartyo, C.-A.-K., Odeberg, J., Djureinovic, D., Takanen, J.O., Hober, S., Alm, T., Edqvist, P.-H., Berling, H., Tegel, H., Mulder, J., Rockberg, J., Nilsson, P., Schwenk, J.M., Hamsten, M., von Feilitzen, K., Forsberg, M., Persson, L., Johansson, F., Zwaalen, M., von Heijne, G., Nielsen, J., Ponten, F., (2015). Tissue-based map of the human proteome. *Science*, **347** <https://doi.org/10.1126/science.1260419>.
- [32]. Kuwahara, M., Hatoko, M., Tada, H., Tanaka, A., (2001). E-cadherin expression in wound healing of mouse skin. *J. Cutan. Pathol.*, **28**, 191–199. <https://doi.org/10.1034/j.1600-0560.2001.028004191.x>.
- [33]. Hunter, M.V., Lee, D.M., Harris, T.J.C., Fernandez-Gonzalez, R., (2015). Polarized E-cadherin endocytosis directs actomyosin remodeling during embryonic wound repair. *J. Cell Biol.*, **210**, 801–816. <https://doi.org/10.1083/jcb.201501076>.
- [34]. Huguenin, M., Müller, E.J., Trachsel-Rösmann, S., Oneda, B., Ambort, D., Sterchi, E.E., Lottaz, D., (2008). The metalloprotease meprin β processes E-cadherin and weakens intercellular adhesion. *PLoS One*, **3**, e2153. <https://doi.org/10.1371/journal.pone.0002153>.
- [35]. Barker, T.H., Engler, A.J., (2017). The provisional matrix: setting the stage for tissue repair outcomes. *Matrix Biol. J. Int. Soc. Matrix Biol.*, **60–61**, 1–4. <https://doi.org/10.1016/j.matbio.2017.04.003>.
- [36]. Hinz, B., (2015). The extracellular matrix and transforming growth factor- β 1: tale of a strained relationship. *Matrix Biol. J. Int. Soc. Matrix Biol.*, **47**, 54–65. <https://doi.org/10.1016/j.matbio.2015.05.006>.
- [37]. Fonta, C.M., Arnoldini, S., Jaramillo, D., Moscaroli, A., Oxenius, A., Behe, M., Vogel, V., (2020). Fibronectin fibers are highly tensed in healthy organs in contrast to tumors and virus-infected lymph nodes. *Matrix Biol. Plus*, **8**, 100046. <https://doi.org/10.1016/j.mbplus.2020.100046>.
- [38]. Bruckner-Tuderman, L., Nilssen, O., Zimmermann, D.R., Dours-Zimmermann, M.T., Kalinke, D.U., Gedde-Dahl, T., Winberg, J.O., (1995). Immunohistochemical and mutation analyses demonstrate that procollagen VII is processed to collagen VII through removal of the NC-2 domain. *J. Cell Biol.*, **131**, 551–559.
- [39]. MEROPS — the Peptidase Database, n.d., <https://www.ebi.ac.uk/merops/cgi-bin/pepsum?id=M12.002;type=P> (accessed March 8, 2021).
- [40]. Guerra, L., Odoriso, T., Zambruno, G., Castiglia, D., (2017). Stromal microenvironment in type VII collagen-deficient skin: the ground for squamous cell carcinoma development. *Matrix Biol. J. Int. Soc. Matrix Biol.*, <https://doi.org/10.1016/j.matbio.2017.01.002>.
- [41]. Nyström, A., Bruckner-Tuderman, L., (2018). Injury- and inflammation-driven skin fibrosis: the paradigm of epidermolysis bullosa. *Matrix Biol. J. Int. Soc. Matrix Biol.*, **68–69**, 547–560. <https://doi.org/10.1016/j.matbio.2018.01.016>.
- [42]. Nyström, A., Bernasconi, R., Bornert, O., (2018). Therapies for genetic extracellular matrix diseases of the skin. *Matrix Biol. J. Int. Soc. Matrix Biol.*, **71–72**, 330–347. <https://doi.org/10.1016/j.matbio.2017.12.010>.
- [43]. Karmilin, K., Schmitz, C., Kuske, M., Körschgen, H., Olf, M., Meyer, K., Hildebrand, A., Felten, M., Fridrich, S., Yiallourous, I., Becker-Pauly, C., Weiskirchen, R., Jahnhen-Dechent, W., Floehr, J., Stöcker, W., (2019). Mammalian plasma fetuin-B is a selective inhibitor of ovastacin and meprin metalloproteinases. *Sci. Rep.*, **9**, 546. <https://doi.org/10.1038/s41598-018-37024-5>.
- [44]. R. Bernasconi, K. Thriene, E. Romero-Fernández, C. Gretzmeier, T. Kühn, Proinflammatory immunity drives injury-induced fibrosis, n.d.
- [45]. Lucas, T., Waisman, A., Ranjan, R., Roes, J., Krieg, T., Müller, W., Roers, A., Eming, S.A., (2010). Differential roles of macrophages in diverse phases of skin repair. *J. Immunol. Baltim. Md 1950*, **184**, 3964–3977. <https://doi.org/10.4049/jimmunol.0903356>.
- [46]. Malik, A., Kanneganti, T.-D., (2018). Function and regulation of IL-1 α in inflammatory diseases and cancer. *Immunol. Rev.*, **281**, 124–137. <https://doi.org/10.1111/immr.12615>.
- [47]. Biasin, V., Wygrecka, M., Marsh, L.M., Becker-Pauly, C., Brcic, L., Ghanim, B., Klepetko, W., Olschewski, A., Kwapiszewska, G., (2017). Meprin β contributes to collagen deposition in lung fibrosis. *Sci. Rep.*, **7**, 39969. <https://doi.org/10.1038/srep39969>.
- [48]. Arnold, P., Otte, A., Becker-Pauly, C., (2017). Meprin metalloproteases: molecular regulation and function in inflammation and fibrosis. *Biochim. Biophys. Acta, Mol. Cell. Res.*, **1864**, 2096–2104. <https://doi.org/10.1016/j.bbamcr.2017.05.011>.
- [49]. Chen, Y., Xu, D., Yao, J., Wei, Z., Li, S., Gao, X., Cai, W., Mao, N., Jin, F., Li, Y., Zhu, Y., Li, S., Liu, H., Yang, F., Xu, H., (2019). Inhibition of miR-155-5p exerts anti-fibrotic effects in silicotic mice by regulating meprin α . *Mol. Ther. Nucleic Acids*, **19**, 350–360. <https://doi.org/10.1016/j.omtn.2019.11.018>.
- [50]. Xu, T.-J., Wang, Q., Ma, X.-W., Zhang, Z., Zhang, W., Xue, X.-C., Zhang, C., Hao, Q., Li, W.-N., Zhang, Y.-Q., Li, M., (2013). A novel dimeric thymosin beta 4 with enhanced activities accelerates the rate of wound healing. *Drug Des. Dev. Ther.*, **7**, 1075–1088. <https://doi.org/10.2147/DDDT.S50183>.
- [51]. Moali, C., Font, B., Ruggiero, F., Eichenberger, D., Rousselle, P., François, V., Oldberg, Å., Bruckner-Tuderman, L., Hulmes, D.J.S., (2005). Substrate-specific modulation of a multisubstrate proteinase. C-terminal processing of fibrillar procollagens is the only BMP-1-dependent activity to be enhanced by PCPE-1. *J. Biol. Chem.*, **280**, 24188–24194. <https://doi.org/10.1074/jbc.M501486200>.
- [52]. Sprenger, A., Küttner, V., Biniossek, M.L., Gretzmeier, C., Boerries, M., Mack, C., Has, C., Bruckner-Tuderman, L., Dengjel, J., (2010). Comparative quantitation of proteome alterations induced by aging or immortalization in primary

- human fibroblasts and keratinocytes for clinical applications. *Mol. BioSyst.*, **6**, 1579–1582. <https://doi.org/10.1039/c003962d>.
- [53]. Norman, L.P., Jiang, W., Han, X., Saunders, T.L., Bond, J.S., (2003). Targeted disruption of the meprin beta gene in mice leads to underrepresentation of knockout mice and changes in renal gene expression profiles. *Mol. Cell. Biol.*, **23**, 1221–1230. <https://doi.org/10.1128/mcb.23.4.1221-1230.2003>.
- [54]. Banerjee, S., Oneda, B., Yap, L.M., Jewell, D.P., Matters, G.L., Fitzpatrick, L.R., Seibold, F., Sterchi, E.E., Ahmad, T., Lottaz, D., Bond, J.S., (2009). MEP1A allele for meprin A metalloprotease is a susceptibility gene for inflammatory bowel disease. *Mucosal Immunol.*, **2**, 220–231. <https://doi.org/10.1038/mi.2009.3>.
- [55]. Banerjee, S., Jin, G., Bradley, S.G., Matters, G.L., Gailey, R.D., Crisman, J.M., Bond, J.S., (2011). Balance of meprin A and B in mice affects the progression of experimental inflammatory bowel disease. *Am. J. Physiol. Gastrointest. Liver Physiol.*, **300**, G273–G282. <https://doi.org/10.1152/ajpgi.00504.2009>.
- [56]. Kilkenny, C., Browne, W.J., Cuthill, I.C., Emerson, M., Altman, D.G., (2010). Improving bioscience research reporting: the ARRIVE guidelines for reporting animal research. *PLoS Biol.*, **8**, e1000412. <https://doi.org/10.1371/journal.pbio.1000412>.
- [57]. Nyström, A., Thriene, K., Mittapalli, V., Kern, J.S., Kiritsi, D., Dengjel, J., Bruckner-Tuderman, L., (2015). Losartan ameliorates dystrophic epidermolysis bullosa and uncovers new disease mechanisms. *EMBO Mol. Med.*, **7**, 1211–1228. <https://doi.org/10.15252/emmm.201505061>.
- [58]. Kühl, T., Mezger, M., Hausser, I., Handgretinger, R., Bruckner-Tuderman, L., Nyström, A., (2015). High local concentrations of intradermal MSCs restore skin integrity and facilitate wound healing in dystrophic epidermolysis bullosa. *Mol. Ther. J. Am. Soc. Gene Ther.*, **23**, 1368–1379. <https://doi.org/10.1038/mt.2015.58>.
- [59]. Nyström, A., Velati, D., Mittapalli, V.R., Fritsch, A., Kern, J.S., Bruckner-Tuderman, L., (2013). Collagen VII plays a dual role in wound healing. *J. Clin. Invest.*, **123**, 3498–3509. <https://doi.org/10.1172/JCI68127>.
- [60]. Kühl, T., Mezger, M., Hausser, I., Guey, L.T., Handgretinger, R., Bruckner-Tuderman, L., Nyström, A., (2016). Collagen VII Half-life at the dermal-epidermal junction zone: implications for mechanisms and therapy of genodermatoses. *J. Invest. Dermatol.*, **136**, 1116–1123. <https://doi.org/10.1016/j.jid.2016.02.002>.
- [61]. Cianfarani, F., De Domenico, E., Nyström, A., Mastroeni, S., Abeni, D., Baldini, E., Ulisse, S., Uva, P., Bruckner-Tuderman, L., Zambruno, G., Castiglia, D., Odorisio, T., (2019). Decorin counteracts disease progression in mice with recessive dystrophic epidermolysis bullosa. *Matrix Biol. J. Int. Soc. Matrix Biol.*, **81**, 3–16. <https://doi.org/10.1016/j.matbio.2018.12.001>.
- [62]. Bornert, O., Kocher, T., Gretzmeier, C., Liemberger, B., Hainzl, S., Koller, U., Nyström, A., (2019). Generation of rabbit polyclonal human and murine collagen VII monospecific antibodies: a useful tool for dystrophic epidermolysis bullosa therapy studies. *Matrix Biol. Plus.*, **4**, 100017. <https://doi.org/10.1016/j.mbplus.2019.100017>.
- [63]. Bornert, O., Hogervorst, M., Nauroy, P., Bischof, J., Swildens, J., Athanasiou, I., Tufa, S.F., Keene, D.R., Kiritsi, D., Hainzl, S., Murauer, E.M., Marinkovich, M.P., Platenburg, G., Hausser, I., Wally, V., Ritsema, T., Koller, U., Haisma, E.M., Nyström, A., (2020). QR-313, an antisense oligonucleotide, shows therapeutic efficacy for treatment of dominant and recessive dystrophic epidermolysis bullosa: a preclinical study. *J. Invest. Dermatol.*, <https://doi.org/10.1016/j.jid.2020.08.018>.